Metal enhanced fluorescence in rare earth doped plasmonic core–shell nanoparticles

S. Derom, Alice Berthelot, A. Pillonnet, O. Benamara, Anne-Marie Jurdyc, Christian Girard, Gérard Colas des Francs

PAPER • **OPEN ACCESS**

Metal enhanced fluorescence in rare earth doped plasmonic core–shell nanoparticles

To cite this article: S Derom *et al* 2013 *Nanotechnology* **24** 495704

OPEN ACCESS
IOP PUBLISHING NANOTECHNOLOGY
Nanotechnology **24** (2013) 495704 (8pp) doi:10.1088/0957-4484/24/49/495704

Metal enhanced fluorescence in rare earth doped plasmonic core–shell nanoparticles

S Derom[1], A Berthelot[2], A Pillonnet[2], O Benamara[2], A M Jurdyc[2], C Girard[3] and G Colas des Francs[1]

[1] Laboratoire Interdisciplinaire Carnot de Bourgogne (ICB), UMR 6303 CNRS-Université de Bourgogne, 9 Avenue A. Savary, BP 47 870, F-21078 Dijon, France
[2] Institut Lumière Matière, UMR 5306 Université de Lyon 1-CNRS, Université Lyon, Villeurbanne F-69622, France
[3] Centre d'Elaboration de Matériaux et d'Etudes Structurales (CEMES), CNRS, 29 rue J. Marvig, BP 94347, F-31055 Toulouse Cedex 4, France

E-mail: gerard.colas-des-francs@u-bourgogne.fr

Received 23 July 2013, in final form 2 October 2013
Published 14 November 2013
Online at stacks.iop.org/Nano/24/495704

Abstract
We theoretically and numerically investigate metal enhanced fluorescence of plasmonic core–shell nanoparticles doped with rare earth (RE) ions. Particle shape and size are engineered to maximize the average enhancement factor (AEF) of the overall doped shell. We show that the highest enhancement (11 in the visible and 7 in the near-infrared) is achieved by tuning either the dipolar or the quadrupolar particle resonance to the rare earth ion's excitation wavelength. Additionally, the calculated AEFs are compared to experimental data reported in the literature, obtained in similar conditions (plasmon mediated enhancement) or when a metal–RE energy transfer mechanism is involved.

(Some figures may appear in colour only in the online journal)

1. Introduction

Rare earth (RE) ions are widely studied for numerous optical applications such as solar cells [1], optical amplification, and biolabeling [2], but also for photodynamic therapy of cancer [3]. Although they present high quantum efficiencies, they can suffer from low absorption cross-sections [4] (around 10^{-20} cm^2) so that metal enhanced fluorescence (MEF) has been proposed to improve their emission properties.

Metal enhanced spectroscopies rely on excitation and/or emission enhancement by coupling emitters to a plasmonic particle. This has been extensively studied, notably for tip- or surface-enhanced Raman scattering (TERS/SERS) [5] or dye fluorescence enhancement [6, 7]. In practice, the highest signal enhancement is achieved for low initial absorption cross-section *and* quantum yield, since both the excitation and the emission processes are enhanced. Sun *et al* described SERS as photoluminescence enhancement in the limit of null initial absorption cross-section and quantum yield [8]. Therefore, SERS presents the highest enhancement (up to 10^6) [9] whereas MEF is typically of a few tens only [10]. Nevertheless, the results achieved for dye molecules cannot be directly transposed to rare earth ions which present extremely low absorption cross-sections but quantum efficiencies close to unity, in contrast to dyes which present high absorption cross-sections and generally lower quantum efficiencies. In addition, it is worthwhile to note that lanthanide luminescence is also extremely sensitive to the surroundings so that identifying the role of plasmons is a difficult task.

A large number of works, mainly experimental [11–22], but also theoretical [23–25], have been realized in order to probe the possibility to enhance the optical properties of rare earth ions placed near metal nanoparticles. Some recent works have highlighted that gold or silver metal nanoparticles could change the selection rules of rare earth ion emission [16, 26], but the localized plasmon contribution remains under discussion. Indeed, it is very difficult to separate the respective roles of plasmons and energy transfer in the observed enhancement

of RE ion luminescence [27]. Plasmon mediated enhancement relies on the antenna effect which increases the excitation field and/or radiative emission rate [28], whereas energy transfer is a dipole–dipole Förster-like mechanism between the metal nanocrystal (donor or sensitizer) and the RE ions (acceptor) [11]. It has been observed that energy transfer is at the origin of luminescence enhancement near small gold and silver clusters composed of a few atoms (crystal size of a few nm) [27, 29]. However, larger metal particles (typically a few tens of nm) are generally preferred for plasmon-enhanced fluorescence [14, 18–20, 22]. Recently, Ma *et al* measured three-fold and 24-fold enhancement factors for Eu^{3+} doped silver core–shell nanoparticles with 20 nm core/15 nm shell and 9 nm core/11 nm shell, respectively [15]. However, they used an excitation wavelength of $\lambda_{exc} = 260$ nm, far from the dipolar resonance, so that we think that the enhancement mechanism is different from plasmon-enhanced spectroscopy and most likely originates from energy transfer. Two other groups have reported three-fold enhancement for Eu^{3+} ions coupled to about 30 nm silver particles when excited close to the silver dipolar resonance [19, 22]. In a former work, Malta and Couto dos Santos have made a rough estimation of the possible emission enhancement for europium ion doped glasses containing silver nanoparticles [23]. They estimated up to 50-fold maximum *local* enhancement factor for 30 nm silver particles but did not conclude about the global enhancement of the overall doped shell.

The purpose of this work is to theoretically determine and optimize the plasmon contribution to the luminescence enhancement in plasmonic nanoparticles doped with lanthanides. Particular attention is devoted to the description of an ensemble of rare earth ions coupled to a metallic nanoparticle instead of a single emitter coupled to one particle as generally done since we are interested in the optical response of the whole doped nanostructure. Firstly, we investigate the role of the localized plasmons supported by the nanoparticle and determine the optimal particle resonance position compared to the emitter absorption and emission peak. To this end, we define in section 2 the average fluorescence factor for a doped plasmonic core–shell particle of arbitrary shape. For comparison purposes, we illustrate the enhancement mechanism by considering a laser dye, namely Rhodamine 6G (Rh6G), coupled to a spherical metal particle [30]. Secondly, in section 3, we investigate the fluorescence enhancement for rare earth ions emitting in the visible or the near-infrared and placed in the shells of core–shell particles with metal cores. We will thus estimate the achievable plasmonic enhancement.

2. Surface-enhanced fluorescence

In this section, we derive a general expression for the average fluorescent enhancement factor (AEF) near a metal particle. To this aim, we extend the work of Liaw *et al* [31] to an arbitrary geometry. We first derive a closed form expression for the enhancement factor $\alpha(\mathbf{r})$ for randomly oriented emitters near a metal particle. The AEF is then achieved by numerically averaging $\alpha(\mathbf{r})$ over the doped shell volume.

2.1. Enhancement factor of randomly oriented emitters

Let us first consider a single fluorescent system with a transition dipolar moment of arbitrary orientation $\mathbf{p} = p_0(\sin\alpha\cos\beta, \sin\alpha\sin\beta, \cos\alpha)$ and intrinsic quantum yield η_0. If the incident field is $\mathbf{E}_0$, the fluorescent signal in the absence of a plasmonic particle is $p_0^2 |\mathbf{E}_0|^2 \eta_0$. The plasmonic particle modifies

- the excitation rate $\pi(\mathbf{r}, \omega_{exc}) = |\mathbf{p}\cdot\mathbf{E}(\mathbf{r}, \omega_{exc})|^2 / p_0^2 |\mathbf{E}_0|^2$, where $\mathbf{E}(\mathbf{r}, \omega_{exc})$ refers to the excitation field at the emitter location $\mathbf{r}$ and excitation angular frequency ω_{exc},
- and the emitter quantum yield $\eta(\mathbf{r}, \omega_{em}) = \gamma^{rad}/(\gamma^{rad} + \gamma^{NR})$ at the emission angular frequency ω_{em}.

As an example, we present in figure 1 the excitation and decay rates calculated for an emitter close to a gold or silver bead. The emitter is perpendicular to the particle surface since stronger effects are expected for this orientation. The excitation and radiative rates follow the dipolar plasmon mode dispersion for small particle diameters. Large particles support a leaky quadrupolar mode so that the radiative rate couples to this mode. Note that the excitation rate weakly follows the quadrupolar mode dispersion since the emitter is not located on a mode lobe. Finally, the non-radiative rate originates from coupling to high order modes so that it presents a flat dispersion curve [33]. The low order modes are well-separated in the case of a silver particle due to lower losses (compare the non-radiative rates near gold and silver structures). Lastly, we observe that the dipolar plasmon resonance can be tuned from $\lambda = 525$ nm (well-defined resonance) to $\lambda \approx 900$ nm (large resonance) for gold bead diameters varying from $D = 10$ to 200 nm. For silver nanoparticle diameters between 10 and 100 nm, the dipolar resonance wavelength varies from $\lambda = 400$ to 530 nm.

Finally, both the excitation and the emission rates depend on the emitter location and orientation in the presence of plasmonic nanostructures. The enhancement factor is expressed as

$$\alpha_{\mathbf{p}}(\mathbf{r}, \omega_{exc}, \omega_{em}) = \frac{|\mathbf{p}\cdot\mathbf{E}(\mathbf{r}, \omega_{exc})|^2 \, \eta(\mathbf{r}, \omega_{em})}{p_0^2 |\mathbf{E}_0|^2 \eta_0}. \quad (1)$$

In the case of arbitrary orientation, the quantum yield is expressed as [34]

$$\begin{aligned}\eta = {} & \sin^2\alpha\cos^2\beta\,\eta_x + \sin^2\alpha\sin^2\beta\,\eta_y + \cos^2\alpha\,\eta_z \\ & + \sin^2\alpha\cos\beta\sin\beta\,\eta_{xy} + \sin\alpha\cos\alpha\cos\beta\,\eta_{xz} \\ & + \sin\alpha\cos\alpha\sin\beta\,\eta_{yz}, \end{aligned} \quad (2)$$

where $\eta_i = \Gamma_{rad,i}/(\Gamma_{rad,i} + \Gamma_{NR,i})$ is the quantum yield associated with the i-orientation ($i = x, y$ or z). The η_{ij} ($i, j = x, y$ or z) refer to crossed-terms that have to be considered for oblique dipole moments (see [34, 35] for details). Assuming randomly oriented emitters at location $\mathbf{r}$, we calculate the mean enhancement factor over all the possible orientations as

$$\begin{aligned}\alpha(\mathbf{r}, \omega_{exc}, \omega_{em}) = {} & \frac{3}{4\pi}\int_{\alpha=0}^{\pi}\int_{\beta=0}^{2\pi} \alpha_{\mathbf{p}}(\mathbf{r}, \omega_{exc}, \omega_{em}) \\ & \times \sin\alpha \, d\alpha \, d\beta, \end{aligned} \quad (3)$$

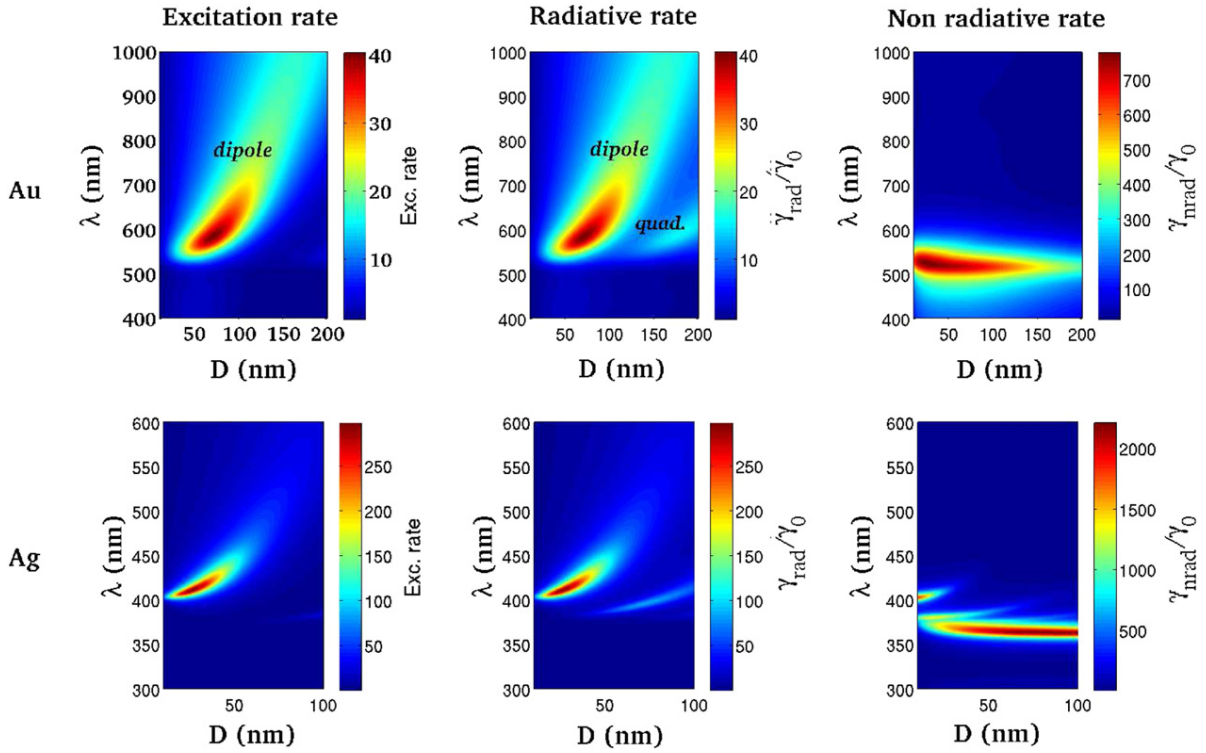

Figure 1. Excitation (left), radiative (middle) and non-radiative (right) rates near a metal spherical particle as a function of wavelength and particle diameter D. The top (bottom) line refers to a gold (silver) particle. The dipolar emitter is located 5 nm from the particle surface and perpendicular to it. The optical index of the embedding matrix is $n = 1.5$. The metal dielectric constants are taken from Johnson and Christy [32].

where the factor 3 ensures a unit enhancement factor for isolated emitters excited with a linearly polarized field. Interestingly enough, the integration over the dipole orientation is analytical. After a little algebra, we achieve

$$\begin{aligned}\alpha(\mathbf{r}, \omega_{\text{exc}}, \omega_{\text{em}}) = &(\eta_x(3E_x^2 + E_y^2 + E_z^2) \\ &+ \eta_y(E_x^2 + 3E_y^2 + E_z^2) \\ &+ \eta_z(E_x^2 + E_y^2 + 3E_z^2)) \\ &\times (5\,|\mathbf{E}_0|^2\,\eta_0)^{-1}. \end{aligned} \quad (4)$$

It is also useful to derive this expression in spherical coordinates, $\mathbf{r} = (r, \theta, \phi)$. With the subscripts $\parallel$ and $\perp$ indicating an orientation parallel or perpendicular to the particle surface, it is written as

$$\begin{aligned}\alpha(\mathbf{r}, \omega_{\text{exc}}, \omega_{\text{em}}) = &(\eta_{\parallel}(2E_r^2 + 4E_\theta^2 + 4E_\phi^2) \\ &+ \eta_{\perp}(3E_r^2 + E_\theta^2 + E_\phi^2)) \\ &\times (5\,|\mathbf{E}_0|^2\,\eta_0)^{-1}, \end{aligned} \quad (5)$$

which leads to an analytical expression for (homogeneous, core–shell or onion-like) spherical particles, thanks to the Mie expansion [36, 37]. In the following, $\alpha(\mathbf{r}, \omega_{\text{exc}}, \omega_{\text{em}})$ is referred to as the local fluorescence enhancement.

Obviously, the choice of the particle size, shape and material depends on the fluorescent system. In the case of dye molecules, with a low Stokes shift between the absorption and emission wavelengths, the most efficient fluorescence enhancement is achieved when the particle dipolar resonance overlaps both the excitation and the emission wavelengths [10, 38]. For instance, let us consider Rhodamine 6G. We will compare rare earth doped nanoparticles to this reference system. The absorption and emission peaks are near $\lambda_{\text{exc}} = 532$ nm and $\lambda_{\text{em}} = 560$ nm, respectively. Figure 2 shows the local fluorescent enhancement for randomly oriented Rh6G molecules dispersed in polymethyl methacrylate (PMMA) near silver spherical particles. The maximum fluorescence enhancement occurs for dye molecules coupled to a 80 nm particle (figure 2(a)). Such a large silver bead supports a dipolar plasmon at about $\lambda \approx 500$ nm with a broad resonance width (and a quadrupolar mode at $\lambda = 400$ nm, see figure 2(c)). Therefore both the excitation field and the radiative rates are significantly enhanced by coupling to the dipolar mode. Meanwhile, the non-radiative rate remains limited due to poor coupling to high order modes that appear at lower wavelength (see also figure 1). Figure 2(b) presents the local enhancement factor calculated near an 80 nm silver sphere. It follows the particle's dipolar mode profile, with a maximum enhancement of $\alpha \approx 18$ slightly shifted from the incident polarization axis [31, 39].

2.2. Layer- and shell-averaged enhancement factors

Finally, the average enhancement factor of the whole doped volume V_0 can be numerically computed as

$$\text{AEF}(\omega_{\text{exc}}, \omega_{\text{em}}) = \frac{1}{V_0} \iiint_{\mathbf{r} \in V_0} \alpha(\mathbf{r}, \omega_{\text{exc}}, \omega_{\text{em}})\, \text{d}V. \quad (6)$$

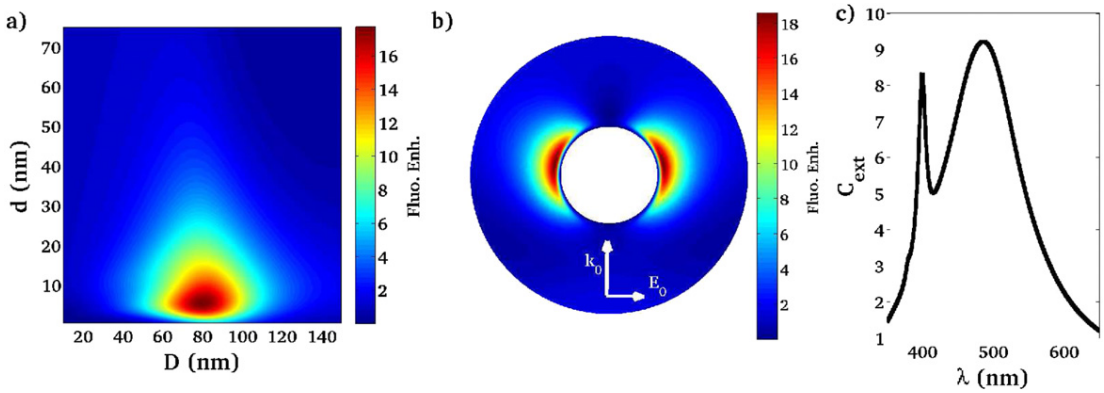

Figure 2. Fluorescence enhancement near a silver particle for randomly oriented molecules. (a) As a function of the particle diameter and dye–particle distance (the molecules are along the incident field polarization axis). (b) Near an 80 nm silver particle. The excitation and emission wavelengths are $\lambda_{exc} = 532$ nm and $\lambda_{em} = 560$ nm, respectively. The embedding medium is PMMA (optical index $n = 1.5$). (c) Extinction efficiency of an 80 nm silver particle.

In the case of spherical particles, it is also useful to define an average enhancement factor associated with a doped shell layer

$$\alpha_{\text{layer}}(\omega_{\text{exc}}, \omega_{\text{em}}, \mathbf{r}) = \frac{1}{4\pi} \int_{\theta=0}^{\pi} \int_{\phi=0}^{2\pi} \alpha(\mathbf{r}, \omega_{\text{exc}}, \omega_{\text{em}}) \times \sin\theta \, \mathrm{d}\theta \, \mathrm{d}\phi. \quad (7)$$

Note that the average and layer fluorescence enhancement factors are normalized with respect to the doped volume so that they do not depend on the RE concentration but rather characterize the SPP mediated fluorescence enhancement.

Figure 3 shows the layer fluorescence enhancement α_{layer} and the average fluorescence factor of the dye-doped core–shell particle. The overall AEF ≈ 4 is optimized given the absorption and emission wavelengths of the dye molecule. This factor takes into account inhomogeneous excitation in the dipolar modes as well as the distance dependence of the emission rate.

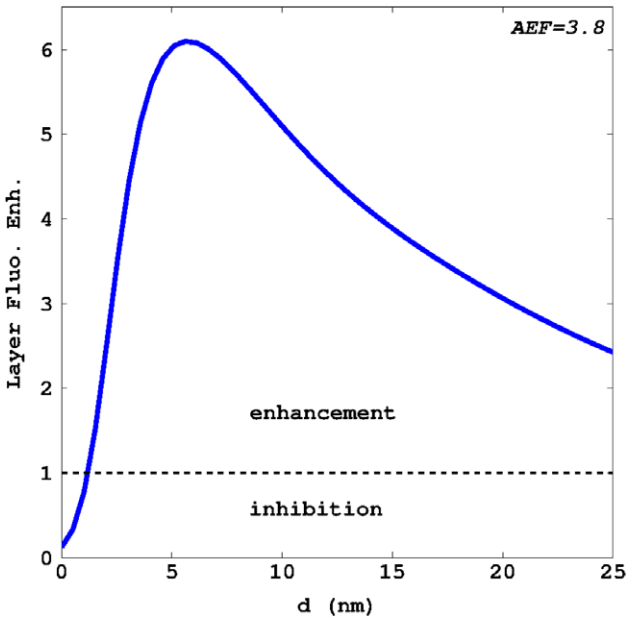

Figure 3. Layer fluorescence enhancement of an Rh6G doped core–shell $Ag@SiO_2$ (silver core 80 nm diameter). The horizontal line indicates the enhancement/inhibition threshold. The average fluorescence enhancement of the whole doped layer (25 nm) is AEF = 3.8.

3. Rare earth doped plasmonic core–shell

In the previous section, we have introduced two important parameters in order to quantify the plasmon/emitter interactions in a core–shell particle: the layer-averaged enhancement factor α_{layer} and the shell-averaged enhancement factor AEF. We have estimated maximum AEF ≈ 4 achievable for an Rh6G doped core–shell $Ag@SiO_2$ reference system. These factors will now allow us to characterize the effect of a metal nanoparticle on the luminescence of RE ions.

In this section, we study the luminescence enhancement for two rare earth ions used in different application domains: Eu^{3+} used, for example, as a biolabel for its emission in the visible spectrum, and Er^{3+}, as the main active medium for amplification at the telecom wavelength, 1.55 μm. Compared to the dye case, the situation could be rather different when considering the fluorescence of rare earth ions. The quantum efficiency of these emitters is close to unity, so plasmon resonance cannot increase this factor much. Lanthanide absorption, based on 4f transitions, in contrast, is very weak (around 10^{-20} cm^2). Therefore, the strongest enhancement is expected when matching the lanthanide absorption wavelength with the dipolar plasmon resonance. The emission of a lanthanide could be far from the excitation wavelength and then probably not much influenced by the plasmon phenomenon [40], in contrast to the previous section where the dye excitation and emission peaks were within the dipolar resonance.

3.1. Emission in the visible

First we consider the europium system: this rare earth ion, usually UV/blue excited, has a maximum emission around 620 nm and a quantum yield close to 1. Since its excitation, corresponding to the $^5D_0$–$^7F_2$ transition, is in the blue part

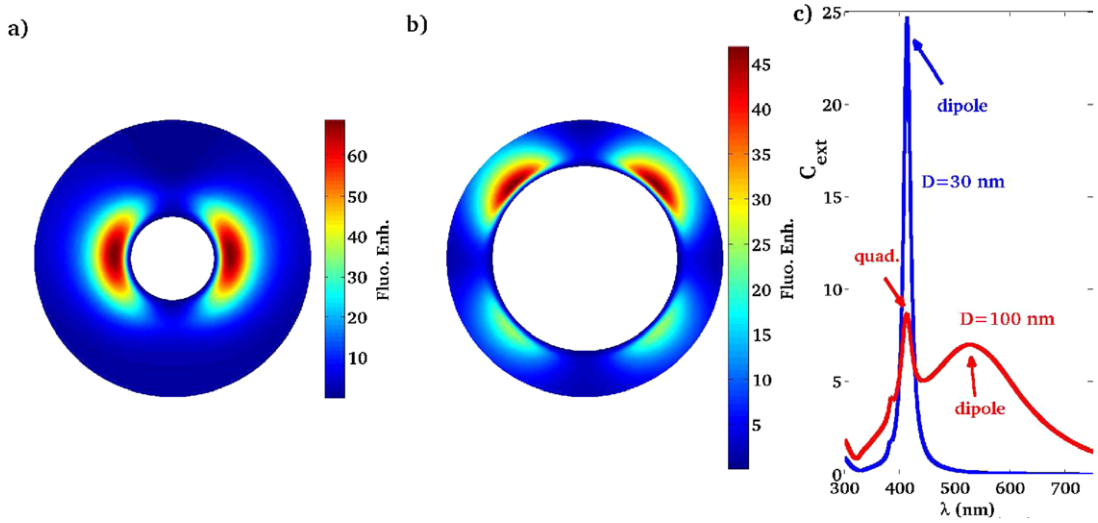

Figure 4. Eu^{3+} fluorescence enhancement near a 30 nm (a) or 100 nm (b) silver particle. (c) Extinction efficiency of a 30 nm (blue line) or 100 nm (red line) silver particle. The dipolar and quadrupolar resonances are indicated for the two particle diameters. The excitation and emission wavelengths are $\lambda_{exc} = 415$ nm and $\lambda_{em} = 620$ nm, respectively. The embedding medium is SiO_2 (optical index $n = 1.5$).

Table 1. Comparison of the excitation and emission rate modifications calculated at the optimum distance for Rh6G and Eu^{3+} doped silver core–shell particles. The local fluorescence enhancement is slightly below the product of the excitation rate × the apparent quantum yield since it obeys equation (5).

	d (nm)	Exc. rate	γ_{rad}/γ_0	γ_{NR}/γ_0	η	Fluo. enh.	AEF
Rh6G–Ag(80 nm)@SiO_2	4	35	9.7	5	0.66	19	3.8
Eu^{3+}–Ag(30 nm)@SiO_2	6	210	1.8	3	0.37	69	11.0
Eu^{3+}–Ag(100 nm)@SiO_2	5.5	90	8.0	4.2	0.66	47	6.7

of the visible spectrum, we have chosen to use silver for the nanoparticle core.

We investigate the Eu^{3+}/silver system in figure 4, where rare earth ions (Eu^{3+}) are included in a dielectric shell and coupled to a silver bead. We consider a silica matrix of the same index as PMMA so that direct comparison with the previous dye molecule case is possible. This luminescent doped core–shell Ag@SiO_2 particle can be chemically synthesized [14, 18, 20]. The excitation and emission wavelengths are $\lambda_{exc} = 415$ nm and $\lambda_{em} = 620$ nm, respectively, corresponding to f–f intra-configurational transitions. As previously, we first determine the size of the metal core that optimizes red luminescence of the europium ions. We find that the maximum local fluorescence enhancement (≈70) is obtained for a 30 nm silver core. We plot in figure 4(a) the map of the fluorescence exaltation achieved near the 30 nm silver sphere. This enhancement is mainly an improvement of the absorption process: we have a strong enhancement of the excitation field resonant with the dipolar resonance of the metal nanoparticle. Since the emission wavelength is far from all the particle resonances (see the extinction efficiency in figure 4(c)), the decay rates are practically not affected by the presence of the plasmonic nanostructure. Table 1 gathers the excitation and decay rates for dye-doped and RE-doped silver core–shell particles. For dye molecules, with small Stokes shifts, large particles lead to a stronger effect since they correspond to large resonances and coupling to the dipolar plasmon enhances both the excitation and the radiative emission rates. In contrast, particles with small metal cores are better candidates to enhance RE emission. This leads to a strong excitation rate increase that compensates the decrease of the apparent quantum yield.

By increasing the metal nanoparticle size, we observe a second optimum size (100 nm) for which efficient enhancement of the europium fluorescent signal occurs (≈50) (figure 4(b)). In this latter case, the excitation field couples to the plasmon quadrupolar mode ($\lambda = 415$ nm) and the radiative rate is also efficiently enhanced by coupling to the dipolar mode ($\lambda \approx 525$ nm, figure 4(c)). This leads to intermediate luminescence enhancement as compared to the dye-doped system and dipolar assisted RE luminescence enhancement (see table 1). In addition, this possibility to enhance the excitation by coupling to the quadrupolar resonance and the emission by coupling to the dipolar resonance offers a supplementary degree of freedom for luminescence control.

Having determined the optimal nanoparticle sizes in order to enhance the red luminescence of a single Eu^{3+} ion, we now estimate the enhancement of an infinitely thin doped shell. Figure 5 shows the evolution of the layer fluorescence enhancement α_{layer} with the distance between the metal and the emitters and the average fluorescence enhancement factor for the whole Eu^{3+} doped shell for these two optimal sizes. For a metal core of 30 nm and a doped shell thickness of 25 nm, we achieve a strong AEF = 11. This high AEF relies on the strong field enhancement at the plasmon dipolar mode

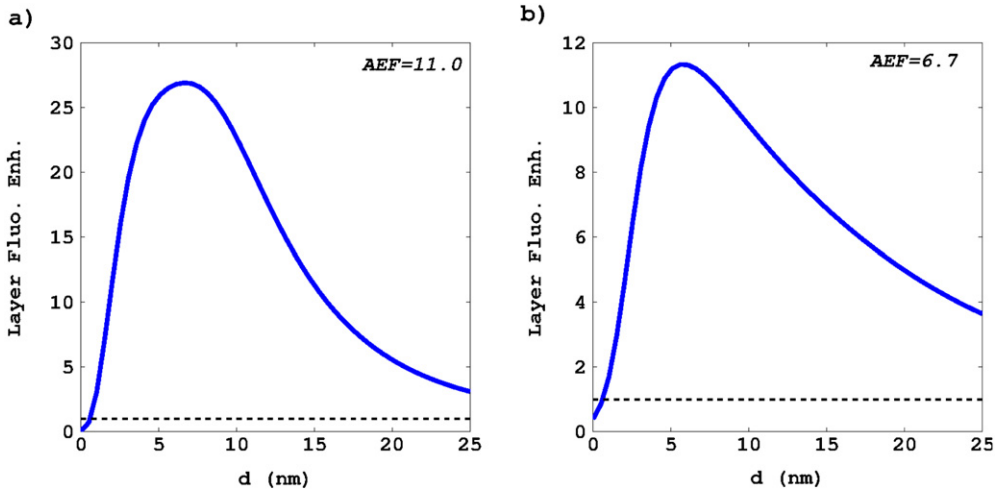

Figure 5. Layer fluorescence enhancement of a Eu^{3+} doped core–shell $Ag@SiO_2$ spherical particle with a silver core of 30 nm (a) or 100 nm (b). The average fluorescence enhancement of the whole doped layer (25 nm) is reported in each figure. The horizontal line indicates the enhancement/inhibition threshold.

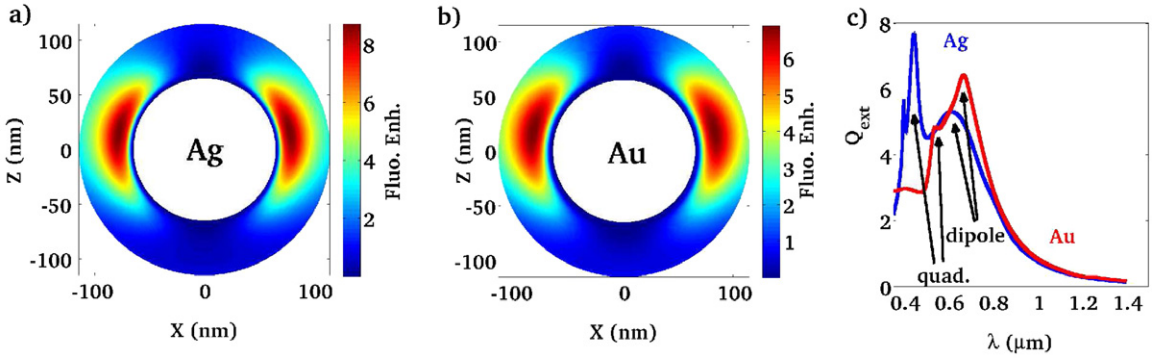

Figure 6. Fluorescence enhancement of randomly oriented Er^{3+} near a 130 nm silver (a) or gold (b) particle. The excitation and emission wavelengths are $\lambda_{exc} = 800$ nm and $\lambda_{em} = 1.55$ μm, respectively. (c) The extinction efficiency of a 130 nm silver (blue line) or gold (red line) particle. The embedding medium is SiO_2 (optical index $n = 1.5$).

resonance. Quenching is limited to emitters very close to the metal surface.

Finally, it is not possible to achieve fluorescence enhancement for these rare earth doped systems using a gold core (even with optimization of the core diameter) since the gold particle's dipolar resonance cannot be tuned to the Eu^{3+} absorption peak, $\lambda = 415$ nm (see figure 1).

3.2. Emission in the near-infrared

3.2.1. Spherical core–shell particle. Erbium ions (Er^{3+}) are widely used for optical amplification for telecom applications since they emit around $\lambda_{em} = 1.55$ μm. We investigate the possibility to enhance their IR emission signal using a core–shell configuration. In an erbium doped fiber amplifier (EDFA), they are usually pumped at 800 or 980 nm wavelength in order to limit the non-radiative losses present with high energy pumping. We consider an excitation wavelength of $\lambda_{exc} = 800$ nm and emission at $\lambda_{em} = 1.55$ μm. We calculate the maximum enhancement of a spherical core–shell particle doped with Er^{3+} for a 130 nm metal core, for either $Ag@SiO_2$ or $Au@SiO_2$. We find a maximum local enhancement of up to 8.5 (6.5) fold near a silver (gold) particle resulting from the excitation of the large dipolar resonance (see figure 6(c)). Our simulation gives then an average enhancement factor of 2.3 (1.7) for the whole doped volume V_0 for a silver (gold) core coated with a 25 nm doped shell layer. This poor AEF is due to the positions of the excitation and emission wavelengths of Er^{3+}, both far from the plasmon maximum. Since it is possible to red shift the longitudinal dipolar plasmon resonance with a nanoparticle presenting a high aspect ratio, we propose to optimize the AEF with an elongated metal core.

3.2.2. Nanorod core–shell particle. Spherical core–shell particles present limited AEF and require one to use large particles in order to red shift the plasmon dipolar resonance to match the Er^{3+} absorption spectrum. Another possibility is to use rod shaped particles with high aspect ratios [12, 41, 42]. In this last section, we investigate core–shell nanorods and estimate the fluorescent enhancement (equations (4) and (6)). To this end, the excitation electric field **E** and emission rates Γ_i

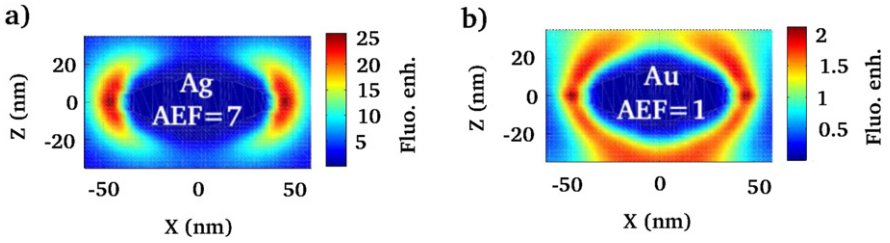

Figure 7. Fluorescence enhancement of randomly oriented Er^{3+} near a silver (a) or gold (b) nanorod (70 nm × 20 nm). The incident electric field is polarized along the rod's long axis. The excitation and emission wavelengths are $\lambda_{exc} = 800$ nm and $\lambda_{em} = 1.55$ μm, respectively. The AEF over the whole (3D) 25 nm doped shell is indicated. The two first nm of the shell are undoped (SiO_2 spacer). The embedding medium is SiO_2 (optical index $n = 1.5$).

need to be evaluated at any location in the doped layer. In the case of an arbitrary structure, they can be calculated thanks to the Green's dyad technique [43–45]. Liaw *et al* investigated similar structures using a multiple multipole method [42]. However, they limited the computation to a plane (the emitter orientation was constrained in two dimensions and only the doped layer inside the plane of incidence was considered). Since the highest fluorescence rate is obtained for these emitter positions and orientations, this leads to overestimation of the enhancement factor of the whole doped layer. Their work, however, paves the way to optimization of the shape of the elongated core–shell particle.

Figure 7(a) represents the fluorescence enhancement near a silver nanorod. The aspect ratio of the rod has been fixed in order to match the particle resonance and the excitation field ($\lambda_{exc} = 800$ nm). The volume of the nanorod is the same as for a 30 nm spherical particle so that the achieved enhancement factor can be compared to the visible regime (figure 4(a)). The tip effect strengthens the field enhancement at the dipolar resonance and we observe a fluorescence enhancement of up to 25 fold near the rod tip. Finally, we achieve an average enhancement factor of AEF = 7 for the whole doped shell, comparable to the visible regime (figure 5). There is no improvement for a gold core (AEF = 1, figure 7(b)) due to high losses. Nevertheless, we would like to mention that we used the dielectric constant of the bulk metal although crystalline nanoparticles present lower losses. This could lead to a small improvement of the enhancement factor.

4. Conclusion

In this work, we have quantified the plasmon contribution to the luminescence enhancement of rare earth doped metallic core–shell nanoparticles. This would therefore help in discriminating and then optimizing the different enhancement mechanisms that could play a role in rare earth doped plasmonic core–shell particles.

The highest plasmon mediated enhancement is achieved when the particle's dipolar resonance matches the excitation wavelength. The enhancement mainly comes from excitation rate enhancement by coupling to the dipolar mode, whereas the emission process is weakly modified. It is also possible to enhance the excitation by coupling to the quadrupolar plasmon and the emission by coupling to the dipolar plasmon. This offers a supplementary degree of freedom for luminescence control. These results differ from dye-doped particles. Indeed, the small Stokes shift between the emission and excitation wavelengths leads then to the choice of a particle resonance overlapping the two in order to enhance both the excitation and the radiative rates by coupling to the dipolar resonance.

We demonstrate average enhancement factors of the fluorescence on the overall RE-doped silver nanoparticle of AEF = 11 and AEF = 7 in the visible and near-infrared regimes, respectively. A gold core leads to a lower effect due to larger losses.

These values are similar to the AEFs measured on RE–metal nanocluster systems [15, 27], where the enhancement originates from energy transfer. Up to 250-fold enhancement has been reported, but probably due to the concentration effect [27]. We, however, envision different applications for RE-doped core–shell plasmonic particles and RE–metal nanoclusters. Colloidal solutions of plasmonic particles can be synthesized and would be useful as, e.g., biolabels or solar cells, whereas RE–nanocluster doped glasses are promising materials for telecom fiber amplification.

Acknowledgments

This work is supported by the Agence Nationale de la Recherche (Fenoptiχs ANR-09-NANO-23 and HYNNA ANR-10-BLAN-1016). Calculations were performed using DSI-CCUB resources (Université de Bourgogne).

References

[1] Timmerman D, Izeddin I, Stallinga P, Yassievich I and Gregorkiewicz T 2008 Space-separated quantum cutting with silicon nanocrystals for photovoltaic applications *Nature Photon.* **2** 105

[2] Bouzigues C, Gacoin T and Alexandrou A 2011 Biological applications of rare-earth based nanoparticles *ACS Nano* **11** 8488

[3] Wang C, Tao H, Cheng L and Liu Z 2011 Near-infrared light induced *in vivo* photodynamic therapy of cancer based on upconversion nanoparticles *Biomaterials* **32** 6145

[4] Bunzli J C, Comby S, Chauvin A S and Vandevyver C 2007 New opportunities for lanthanide luminescence *J. Rare Earths* **25** 257

[5] Pettinger B 2010 Single-molecule surface- and tip-enhanced Raman spectroscopy *Mol. Phys.* **108** 2039–59

[6] Fort E and Grésillon S 2008 Surface enhanced fluorescence *J. Phys. D: Appl. Phys.* **41** 013001

[7] Giannini V, Fernandez-Dominguez A I, Heck S C and Maier S A 2011 Plasmonic nanoantennas: fundamentals and their use in controlling the radiative properties of nanoemitters *Chem. Rev.* **111** 3888–912

[8] Sun G, Khurgin J B and Tsai D P 2012 Comparative analysis of photoluminescence and Raman enhancement by metal nanoparticles *Opt. Lett.* **37** 1583–5

[9] Fang Y, Seong N-H and Dlott D D 2008 Measurement of the distribution of site enhancements in surface-enhanced raman scattering *Science* **321** 388

[10] Bharadwaj P and Novotny L 2007 Spectral dependence of single molecule fluorescence enhancement *Opt. Express* **15** 14266–74

[11] Strohhöfer C and Polman A 2002 Silver as sensitizer for erbium *Appl. Phys. Lett.* **81** 1414

[12] Mertens H and Polman A 2006 Plasmon-enhanced erbium luminescence *Appl. Phys. Lett.* **89** 211107

[13] Marques A C and Almeida R M 2007 Er photoluminescence enhancement in Ag-doped sol–gel planar waveguides *J. Non-Cryst. Solids* **353** 2613–8

[14] Aslan K, Wu M, Lakowicz J R and Geddes C D 2007 Fluorescent core–shell Ag@SiO_2 nanocomposites for metal-enhanced fluorescence and single nanoparticle sensing platforms *J. Am. Chem. Soc.* **129** 1524–5

[15] Ma Z, Dosev D and Kennedy I M 2009 A microemulsion preparation of nanoparticles of europium in silica with luminescence enhancement using silver *Nanotechnology* **20** 085608

[16] Kassab L R P, da Silva D S and de Araújo C B 2010 Influence of metallic nanoparticles on electric-dipole and magnetic-dipole transitions of Eu^{3+} doped germanate glasses *J. Appl. Phys.* **107** 113506

[17] Som T and Karmakar B 2011 Nano silver: antinomy glass hybrid nanocomposites and their enhanced fluorescence application *Solid State Sci.* **13** 887–95

[18] van Wijngaarden J T, van Schooneveld M M, de Mello Donega C and Meijerink A 2011 Enhancement of the decay rate by plasmon coupling for Eu^{3+} in an Au nanoparticle model system *Europhys. Lett.* **93** 57005

[19] Reisfeld R, Saraidarov T, Panzer G, Levchenko V and Gaft M 2011 New optical material europium EDTA complex in polyvinyl pyrrolidone films with fluorescence enhanced by silver plasmons *Opt. Mater.* **34** 351–4

[20] Deng W, Sudheendra L, Zhao J, Fu J, Jin D, Kennedy I M and Goldys E M 2011 Upconversion in $NaYF_4$:Yb, Er nanoparticles amplified by metal nanostructures *Nanotechnology* **22** 325604

[21] Rivera V A G, Ledemi Y, Osorio S P A, Manzani D, Messaddeq Y, Nunes L A O and Marega E Jr 2012 Efficient plasmonic coupling between Er^{3+}:(Ag/Au) in tellurite glasses *J. Non-Cryst. Solids* **358** 399–405

[22] Amjad R, Sahar M, Dousti M, Ghoshal S and Jamaludin M 2013 Surface enhanced Raman scattering and plasmon enhanced fluorescence in zinc-tellurite glass *Opt. Express* **21** 21282–90

[23] Malta O L and Couto dos Santos M A 1990 Theoretical analysis of the fluorescence yield of rare earth ions in glasses containing small metallic particles *Chem. Phys. Lett.* **174** 13–8

[24] Esteban R, Laroche M and Greffet J-J 2009 Influence of metallic nanoparticles on upconversion processes *J. Appl. Phys.* **105** 033107

[25] Fischer S, Hallermann F, Eichelkraut T, von Plessen G, Krämer K W, Biner D, Steinkemper H, Hermle M and Goldschmidt J C 2012 Plasmon enhanced upconversion luminescence near gold nanoparticles-simulation and analysis of the interactions *Opt. Express* **20** 271–82

[26] Karaveli S and Zia R 2011 Spectral tuning by selective enhancement of electric and magnetic dipole emission *Phys. Rev. Lett.* **106** 193004

[27] Eichelbaum M and Rademann K 2009 Plasmonic enhancement or energy transfer? On the luminescence of gold-, silver-, and lanthanide-doped silicate glasses and its potential for light-emitting devices *Adv. Funct. Mater.* **19** 2045–52

[28] Busson M, Rolly B, Stout B, Bonod J W N and Bidault S 2012 Photonic engineering of hybrid metal–organic chromophores *Angew. Chem. Int. Edn* **51** 11083–7

[29] Maurizio C, Trave E, Perotto G, Bello V, Pasqualini D, Mazzoldi P, Battaglin G, Cesca T, Scian C and Mattei G 2011 Enhancement of the Er^{3+} luminescence in Er-doped silica by few-atom metal aggregates *Phys. Rev.* B **83** 195430

[30] Peng B, Zhang Q, Liu X, Ji Y, Demir H, Huan C, Sum T and Xiong Q 2012 Fluorophore-doped core multishell spherical plasmonic nanocavities: resonant energy transfer toward a loss compensation *ACS Nano* **6** 6250–9

[31] Liaw J-W, Liu C-L, Tu W-M, Sun C-S and Kuo M-K 2010 Average enhancement factor of molecules-doped coreshell (Ag@SiO_2) on fluorescence *Opt. Express* **18** 12788–97

[32] Johnson P and Christy R 1972 Optical constants of the noble metals *Phys. Rev.* B **6** 4370–9

[33] Colas des Francs G, Bouhelier A, Finot E, Weeber J-C, Dereux A, Girard C and Dujardin E 2008 Fluorescence relaxation in the near-field of a mesoscopic metallic particle: distance dependence and role of plasmon modes *Opt. Express* **16** 17654–66

[34] Colas des Francs G, Girard C and Dereux A 2002 Theory of near-field optical imaging with a single molecule as a light source *J. Chem. Phys.* **117** 4659–66

[35] Lévêque G *et al* 2002 Polarization state of the optical near-field *Phys. Rev.* E **65** 36701

[36] Kim Y S, Leung P T and George T F 1988 Classical decay rates for molecules in the presence of a spherical surface: a complete treatment *Surf. Sci.* **195** 1–14

[37] Sinzig J and Quinten M 1994 Scattering and absorption by spherical multilayer particles *Appl. Phys.* A **58** 157–62

[38] Reineck V, Gómez D, Ng S, Karg M, Bell T, Mulvaney P and Bach U 2013 Distance and wavelength dependent quenching of molecular fluorescence by Au@SiO_2 core–shell nanoparticles *ACS Nano* **7** 6636

[39] Härtling T, Reichenbach P and Eng L M 2007 Near-field coupling of a single fluorescent molecule and a spherical gold nanoparticle *Opt. Express* **15** 12806–17

[40] Pillonnet A, Berthelot A, Pereira A, Benamara O, Derom S, Colas des Francs G and Jurdyc A-M 2012 Coupling distance between Eu^{3+} emitters and Ag nanoparticles *Appl. Phys. Lett.* **100** 153115

[41] Mertens H and Polman A 2009 Strong luminescence quantum-efficiency enhancement near prolate metal nanoparticles: dipolar versus higher-order modes *J. Appl. Phys.* **105** 44302

[42] Liaw J-W and Tsai H-Y 2012 Theoretical investigation of plasmonic enhancement of silica-coated gold nanorod on molecular fluorescence *J. Quant. Spectrosc. Radiat. Transfer* **113** 470–9

[43] Girard C 2005 Near-field in nanostructures *Rep. Prog. Phys.* **68** 1883–933

[44] Baffou G, Girard C, Dujardin E, Colas des Francs G and Martin O 2008 Molecular quenching and relaxation in a plasmonic tunable system *Phys. Rev.* B **77** 121101(R)

[45] Girard C, Dujardin E, Baffou G and Quidant R 2008 Shaping and manipulation of light fields with bottom-up plasmonic structures *New J. Phys.* **10** 105016